Desalination and Water Treatment
www.deswater.com
doi: 10.5004/dwt.2020.25862

194 (2020) 269–279
August

Application of magnetic peanut husk for methylene blue adsorption in batch mode

Aaron Albert Aryee, Ruize Zhang, Haifang Liu, Runping Han*, Zhaohui Li*, Lingbo Qu*

College of Chemistry, Zhengzhou University, No. 100 of Kexue Road, Zhengzhou 450001, China, Tel. +86 371 67781757; Fax: +86 371 67781556; emails: rphan67@zzu.edu.cn (R. Han), zhaohui.li@zzu.edu.cn (Z. Li), qulingbo@zzu.edu.cn (L. Qu), a.niiayi@yahoo.com (A.A. Aryee), 690724768@qq.com (R. Zhang), 576003731@qq.com (H. Liu)

Received 13 October 2019; Accepted 17 March 2020

ABSTRACT

Magnetic peanut husk (PN-Fe_3O_4) was prepared by co-precipitation and applied for the removal of methylene blue (MB) from the solution. The results from the characterization of PN-Fe_3O_4 showed that Fe_3O_4 was successfully loaded onto peanut husk. The effect of factors such as pH, temperature, salt, and contact time on the adsorption process were carried out using the batch method. The adsorption isotherm was well-described by the Langmuir isotherm whereas the pseudo-second kinetic-order was observed to be the best fitted kinetic model. The maximum equilibrium capacity of PN-Fe_3O_4 according to the Langmuir model was 32.5 mg g^{-1} at 303 K. After three adsorption cycles, PN-Fe_3O_4 had significant adsorption capacities as well as its magnetic properties which ensures its easy separation from the aqueous solution by the use of a magnet. A single-stage batch design for MB adsorption was also presented based on the Langmuir isotherm model. PN-Fe_3O_4 is promising as an adsorbent to remove dyes from the solution.

Keywords: Adsorption; Magnetic peanut husk; Methylene blue; Regeneration

1. Introduction

The pollution of water bodies with industrial effluents has been a source of concern in recent times due to the significant role water plays in the survival of living organisms [1,2]. The constituents of these effluents may include dyes, pesticides, heavy metals, and polycyclic aromatic hydrocarbons [3,4]. Synthetic dyes such as methylene blue (MB) are used extensively in industries such as the textile and paper industry hence may be found in industrial wastewater [1,5].

MB is a cationic dye that has found its application as a coloring agent in the textile industry as well as in medicine. It has also been associated with some adverse effects such as irritation to the skin and when ingested can cause convulsions, diarrhea, nausea, and vomiting [6]. Also, its presence in water affects its aesthetics and makes it undesirable hence the need for its removal from effluents before it is released into the environment.

Activated carbon has been the preferred adsorbent in the adsorption processes for the removal of such pollutants from wastewater due to its excellent adsorption capabilities [7,8]. However, the high cost of commercial activated carbon, the difficulty associated with its removal after the process as well as high regeneration cost act as major drawbacks to its application [9].

In the past decade, agricultural waste materials (AWM) have been observed to be good candidates for use as adsorbents in the removal of pollutants. AWM are found in abundance (hence their low cost) and also, usually require

* Corresponding authors.

facile preparation methods for use as adsorbents [10–13]. These materials are also known to possess functional groups such as –OH and –COOH which enables their surface to be modified to enhance their adsorption capacities as well as minimizing some adverse effects associated with their use [14]. Although significant adsorption capacities have been observed for these AWM, their removal after the adsorption process (involved centrifuging and filtration methods) have been a challenge [15–17].

Review articles in this area in a bid to resolve this challenge observed that the incorporation of magnetic nanoparticles into AWM are able to surmount this challenge as they can easily be separated from the aqueous solution by an applied external magnetic force [18]. Thus, the introduction of magnetic materials into AWM can greatly reduce energy consumption during the adsorption process [19]. Characteristics of a good adsorbent such as good dispersibility, easy functionalization, and good biocompatibility have been observed for some magnetic materials [20,21]. Magnetic materials can be separated from the solution using external magnets hence have good prospects in their application as adsorbents in environmental water treatment [22,23].

In this regard, the co-precipitation method has been the most widely used method for the preparation of Fe_3O_4 nanoparticles [23]. This preparation method can proceed under benign conditions hence it is environmentally friendly. This study, therefore, seeks to incorporate magnetic nanoparticles into AWM via co-precipitation method with the view to overcoming some challenges associated with the synthesis of adsorbents as well as to expound the potential of these materials as adsorbents for practical purposes.

Peanut husk (*Arachis hypogaea*) is generated as waste material in significant quantities due to the large scale production of peanut globally. Thus in this study, a magnetic adsorbent, PN-Fe_3O_4 based on peanut husk was synthesized by incorporating Fe_3O_4 particles into peanut husk and then applied as an adsorbent for the removal of MB from solution. This synthesis design fits into the concept of using "waste to treat waste" as well as offering some added advantages such as facile preparation method under benign environmental conditions and easy separation after the adsorption process.

Studies to assess the effects of experimental conditions such as temperature, contact time, pH, and salt on the adsorption of MB onto the magnetically modified adsorbent (PN-Fe_3O_4) were also assessed.

2. Materials and method

2.1. Materials

Peanut husk (PN) was collected from its natural habitats in the farmland, Luoyang City, China. The biomaterial was washed with tap water and distilled water, dried in an oven at 80°C for 2 h. Dry materials were crushed into powder and sieved to −20 and +40 mesh size, then preserved for use. All chemicals are of analytical grade.

A stock solution of MB (1,000 mg L^{-1}) was prepared by dissolving 1 g of MB in 1,000 mL of distilled water. Working solutions were obtained by diluting the stock solution with distilled water to the desired concentration.

2.2. Preparation of adsorbent and MB solution

The magnetic particle was prepared by co-precipitation [24]. Briefly, 4.80 g of $FeSO_4{\cdot}7H_2O$ and 9.34 g of $FeCl_3{\cdot}6\ H_2O$ (molar ratio of Fe^{2+}:Fe^{3+} as 1:2) were dissolved in 50 mL distilled water. This solution was added slowly to the peanut husk while stirring. The mixture was then placed in a water bath and the temperature was raised to 65°C. An aliquot of ammonia solution (28%) was added to the mixture to precipitate Fe_3O_4 ions. The pH of the mixture was then adjusted to 9.6 by the dropwise addition of ammonia solution. Then after, the mixture was placed in the water bath at 65°C for another 30 min. The mixture was then allowed to cool and the product formed was collected by the use of a magnet. The final product was then washed several times with water and ethanol until the pH was almost 7.0. The obtained product was then dried in an oven at 60°C and then labeled as PN-Fe_3O_4.

2.3. Characterization of adsorbent

The morphology of the unmodified (PN) and modified adsorbents (PN-Fe_3O_4) were obtained by scanning electron microscopy (SEM, Hitachi Su8020, Japan). The Fourier transform infrared microscopy (FTIR) of PN-Fe_3O_4 and PN-Fe_3O_4-MB (after adsorption) were assessed using the FTIR instrument (PE-1710 FTIR). The X-ray photoelectron spectroscopy (XPS, Thermo Escalab 250Xi, England) was carried out to confirm the adsorption mechanism whereas the Squid vibrating sample magnetometer (Quantum Design PPMS DynaCool, North-America) was used to test the magnetization of PN-Fe_3O_4.

2.4. Adsorption experiments

Adsorption experiments to assess the adsorption capacity of the prepared adsorbent (PN-Fe_3O_4) for the removal of MB were carried out using the batch method. Factors such as pH, adsorbent dose, initial MB concentration, temperature, and effect of salt were also carried out. The batch adsorption experiments were done in a mechanical shaker at a speed of 120 rpm. For the adsorption experiment, 10 mL of MB solution (at different concentrations and pH values) were mixed with 0.010 g of the adsorbent in a 50 mL conical flask and then shaken at different contact times.

To assess the effect of a given factor on adsorption, its variable was varied in different experiments whereas all other parameters were kept constant. After the adsorption experiment, PN-Fe_3O_4 was separated from the mixture by the use of a magnet, and the concentration of MB solution measured using a UV/vis-3000 spectrophotometer (Shimadzu UV3000 UV-3000 with a 1 cm path length, Japan) according to the Beer–Lambert law at a maximum wavelength of 665 nm.

The quantity of MB loaded onto a unit mass of PN-Fe_3O_4 (q_t or q_e, mg g^{-1}) was obtained using the expression:

$$q = \frac{V\left(C_0 - C\right)}{m} \tag{1}$$

where C_0 is the initial MB concentration (mg L^{-1}), C_e is the MB concentration at any time t or equilibrium (mg L^{-1}), V is the volume of MB solution (L), and m is the mass of PN-Fe_3O_4 (g).

2.5. Desorption and regeneration

The spent adsorbent (PN–Fe_3O_4–MB) was obtained for the adsorption of 300 mg L^{-1} MB at pH 10. Then, the spent adsorbent was washed with distilled water to remove any unabsorbed dye and was dried at 333 K. MB-loaded PN–Fe_3O_4 was desorbed by a 0.1 mol L^{-1} HCl solution (pH = 1), and the regenerated adsorbent reused under the same experimental conditions. The regeneration efficiency (%) was obtained as the ratio of values of q_e before and after regeneration.

3. Results and discussion

3.1. Characterization

3.1.1. FTIR analysis

The use of the FTIR technique has been observed to be an important tool in the determination of functional groups which may contribute significantly to the adsorption process. Fig. 1 shows the FTIR spectra of PN-Fe_3O_4 before and after adsorption of MB (PN-Fe_3O_4-MB). The peak observed at 3,439 cm^{-1} could be attributed to the O–H stretching whereas that at 587 cm^{-1} could be attributed to the Fe–O bond which signifies the successful formation of magnetic PN-Fe_3O_4 adsorbent [25]. Peaks at 1,632 and 1,635 cm^{-1} indicate C=C stretching in PN-Fe_3O_4 before and after adsorption of MB, respectively. The abundance of these hydroxyl groups may function as proton donors hence in the deprotonated form, they may be involved in the coordination with cationic dyes [9]. The FTIR spectrum of PN-Fe_3O_4 after the adsorption process indicated a shift in the peak of the O–H group to 3,463 cm^{-1}. This occurrence confirms that the O–H bond was involved in the adsorption of MB. The peak at 587 cm^{-1} which was attributed to the Fe–O bond was still observed in the adsorbent after the adsorption process. This result suggests that PN-Fe_3O_4 still possessed its magnetic properties after the adsorption process.

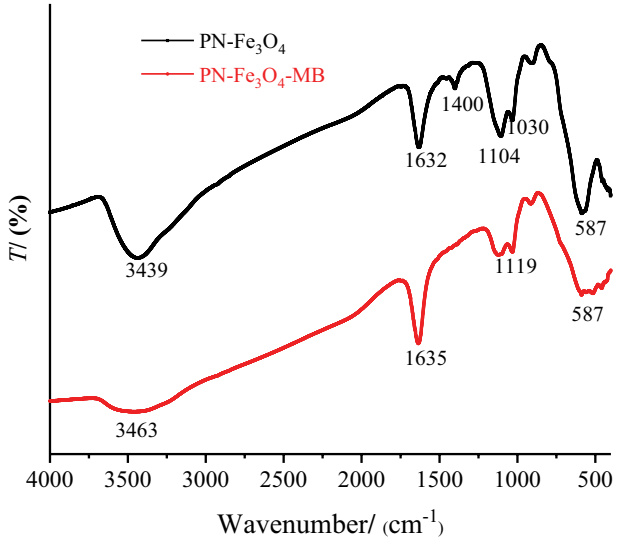

Fig. 1. Comparison of the FTIR spectrum of PN-Fe_3O_4 before and after adsorption of MB.

3.1.2. VSM analysis

The magnetic hysteresis curves of Fe_3O_4 nanoparticles and PN-Fe_3O_4 are presented in Fig. 2. The magnetization saturation values were observed to be 77.64 and 32.74 emu g^{-1} for Fe_3O_4 and PN-Fe_3O_4, respectively. The decrease in the magnetization saturation value of PN-Fe_3O_4 as compared to that of Fe_3O_4 could be due to the magnetic fielding effect of the natural peanut husk. This result confirms the magnetic properties of PN-Fe_3O_4 hence its ability to be easily separated from aqueous solutions by the use of a magnet.

3.1.3. SEM analysis

Fig. 3 shows characterization results obtained from SEM analysis of raw PN and PN-Fe_3O_4. The morphology of PN was observed to be fibrous with a porous and rougher surface. The surface of PN-Fe_3O_4, on the other hand, was observed to be less rough albeit with some observable pores. This observation is attributed to the incorporation of Fe_3O_4 which attaches itself within the pores and the surface of PN. This change in the surface properties also confirms the successful formation of PN-Fe_3O_4. These properties of PN-Fe_3O_4 coupled with its particle size of about 100 μm aids in its adsorption capabilities for the removal of pollutants in wastewater.

3.1.4. XPS analysis

From the XPS results shown in Fig. 4, analysis of the two spectra indicated that the valence states of Fe and O in the adsorbent before adsorption (PN-Fe_3O_4) and after adsorption (PN-Fe_3O_4-MB) demonstrated consistent results. In the O1s spectrum, the Fe–O peak was observed at 529.6 and 532.6 eV in PN-Fe_3O_4 and PN-Fe_3O_4-MB, respectively, indicating the presence of Fe_3O_4 [26]. This shows that the adsorbent still retained its magnetic properties even after adsorption hence could be separated from the aqueous solution using a magnet. The peak at 710.8 eV was observed in the Fe2p spectrum of both Fe_3O_4 and PN-Fe_3O_4,

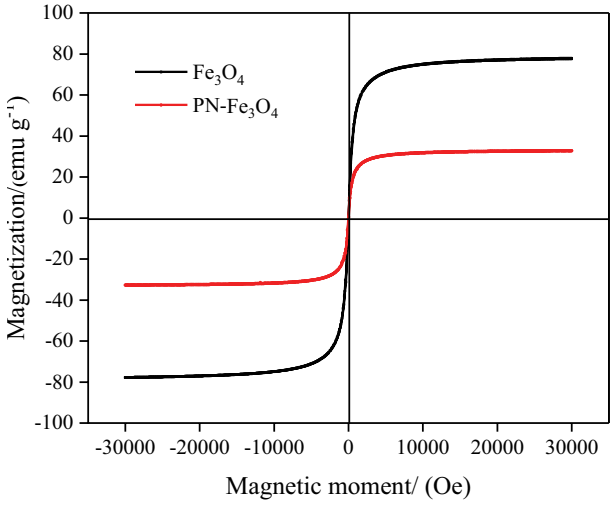

Fig. 2. Hysterical curves of Fe_3O_4 and PN-Fe_3O_4.

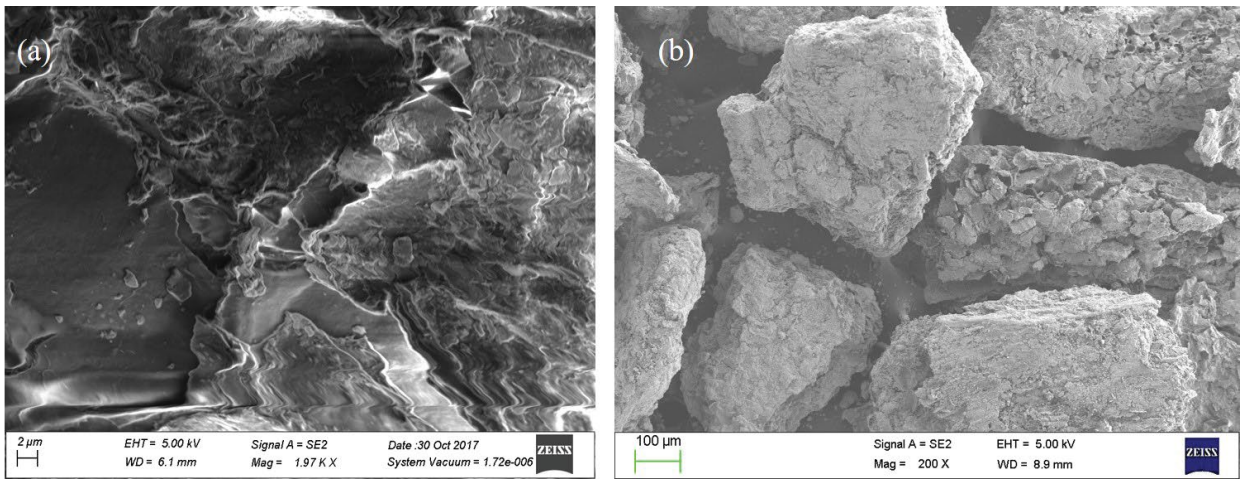

Fig. 3. SEM images of (a) PN and (b) PN-Fe_3O_4.

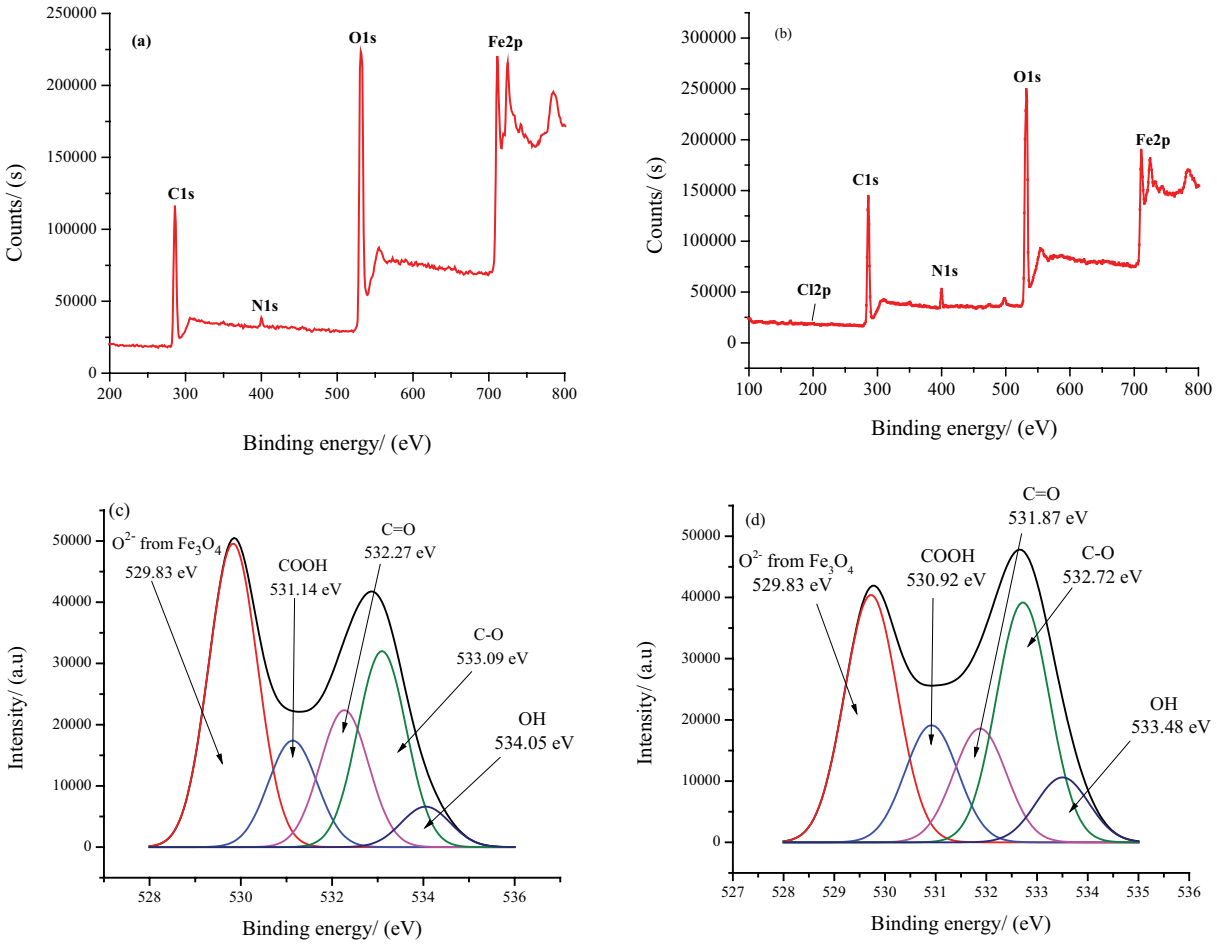

Fig. 4. XPS spectrum of (a) PN-Fe_3O_4 and (b) PN-Fe_3O_4-MB. High-resolution spectrum of O1s (c) before and (d) after the adsorption of MB.

representing Fe $2p_{3/2}$ of ferric species in magnetite [27]. After MB adsorption, the peak of N1s became relatively intense due to the nitrogen element which existed in MB structure.

Fig. 4c and d show the high-resolution peaks of O1s before and after the adsorption process. Analysis of the O1s peak showed that there was about an 18.2% reduction in the O/C molar ratio after the adsorption of MB onto

PN-Fe_3O_4 (i.e., from 95.3% to 77.1%). This observation may be attributed to the interaction between the adsorbed MB ions and the hydroxyl oxygen groups present on PN-Fe_3O_4. Also, there was a redshift in the binding energy of the peaks after the adsorption process. This observation suggests the significant role of electrostatic interactions in the adsorption process [28].

3.2. Adsorption test

3.2.1. Effect of pH and reaction mechanism

The pH of a solution has been observed to be an important factor in the overall adsorption process as it affects the surface charge of the adsorbent, the dissociation of its functional group as well as the chemistry of the solution. As shown in Fig. 5a, it could be seen that the adsorption capacity (q_e) of the adsorbent (i.e., PN-Fe_3O_4) for the removal of MB in solution was strongly influenced by the pH of the solution. The values of q_e were observed to increase with an increase in pH with the maximum recorded at a pH of 10. This phenomenon demonstrates that ion exchange is one dominant factor in the adsorption process [21,22]. A similar trend was observed by Zhou et al. [25] in their study of the removal of Cd(II) from water using iminodiacetic acid-modified magnetic biochar.

The point of zero charge (pzc) is the pH at which the total surface charge on an adsorbent is zero. At pH < pHpzc, the surface of PN-Fe_3O_4 is positively charged hence does not favor the adsorption of MB due to the electrostatic repulsion between the charges and also due to competition with protons for adsorption sites. However, at pH > pHpzc the surface becomes negative hence the higher tendency for the removal of MB. From Fig. 5b, the pzc of PN-Fe_3O_4 was approximately 5.5, thus the pH values should be maintained above this value in order to ensure a negatively charged surface. This condition will be in favor of the adsorption process by electrostatic attraction between PN-Fe_3O_4 and the MB cationic ions. The surface of PN-Fe_3O_4 is endowed with –OH and –COOH functional groups which aid in the adsorption process as expressed below:

$$–Fe–O–(C=O)–(OH)n + MB^+ \rightarrow –Fe–O–(C=O)–(O–MB)n^+ + nH^+ \quad (2)$$

$$–Fe–O–(OH)n + MB^+ \rightarrow –Fe–O–(O–MB)n^+ + nH^+ \quad (3)$$

As recorded by Volesky [29] the pKa values of –COOH and –OH are 1.7–4.7 and 9.8–13, respectively. Due to the difference in their pKa values, the participation of these functional groups is significantly influenced by the solution pH. From the results obtained from the study on the effect of pH on the adsorption process, it can be concluded that the adsorption of MB onto PN-Fe_3O_4 is more likely to be due to the interaction between the –OH groups and that of MB as higher solution pH favors the adsorption process. This observation confirms that the electrostatic interaction may be the underlying reaction mechanism for this adsorption process. Fig. 6 is a schematic diagram showing the plausible reaction mechanism associated with the adsorption of MB onto PN-Fe_3O_4. Maybe another action such as hydrogen bond has existed during the adsorption process and it is not shown in Fig. 6.

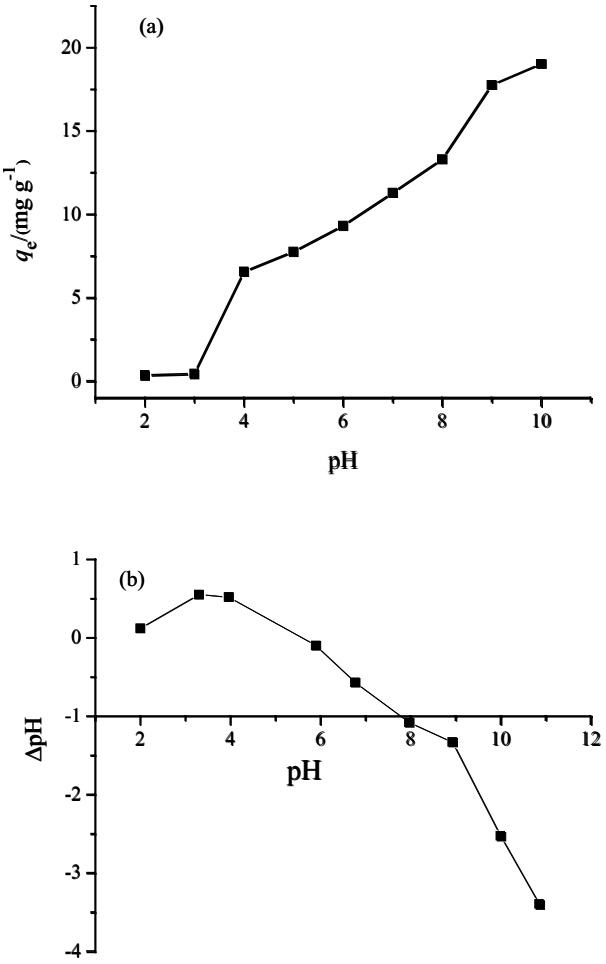

Fig. 5. (a) Effect of initial pH on adsorption of MB (C_0 =100 mg L^{-1}; m = 0.01 g, T= 298 K, t = 4 h) and (b) Plot for determination pH of point zero charge of PN-Fe_3O_4.

3.2.2. Effect of adsorbent dose and different adsorbents

As shown in Fig. 7, the adsorption capacity (q_e) was observed to decrease with an increase in adsorbent dose. This is due to the availability of more active sites for adsorption leading to the unsaturation of these sites. The q_e of PN-Fe_3O_4 was compared to that of raw peanut husk (PN) and Fe_3O_4. Using the batch experiment method (adsorbent dose = 0.01 g, T = 303 K, and contact time = 8 h) the q_e at equilibrium for PN-Fe_3O_4, PN, and Fe_3O_4 for the removal of MB (10 mL, 300 mg L^{-1}, and pH = 10) were found to be 31.9, 37.8, and 17.2 mg g^{-1}, respectively. The reduction in the q_e of PN-Fe_3O_4 for the removal of MB as compared to that of PN could be attributed to the presence of Fe_3O_4 which reduces the active sites available for the attachment of MB. However, the magnetic property of PN-Fe_3O_4 enables it to be easily separated from the solution after the adsorption process with a negligible loss in its quantity as compared to that of PN.

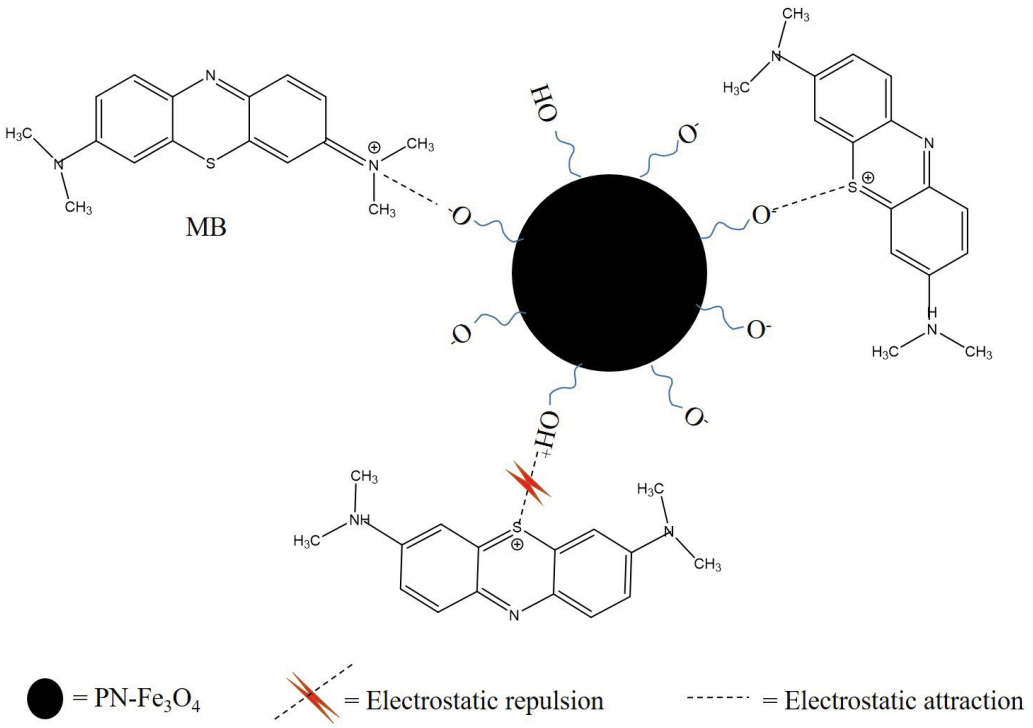

Fig. 6. Schematic diagram showing the plausible reaction mechanism for adsorption of MB onto PN-Fe_3O_4.

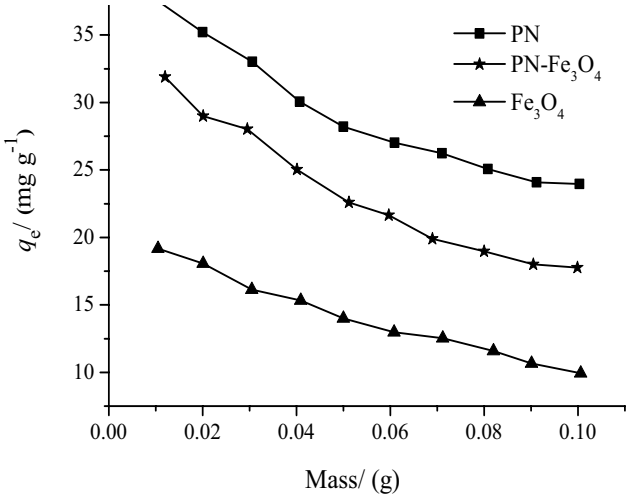

Fig. 7. Adsorption of MB onto different adsorbents (T = 303 K, t = 8 h, C_0 =300 mg L^{-1}).

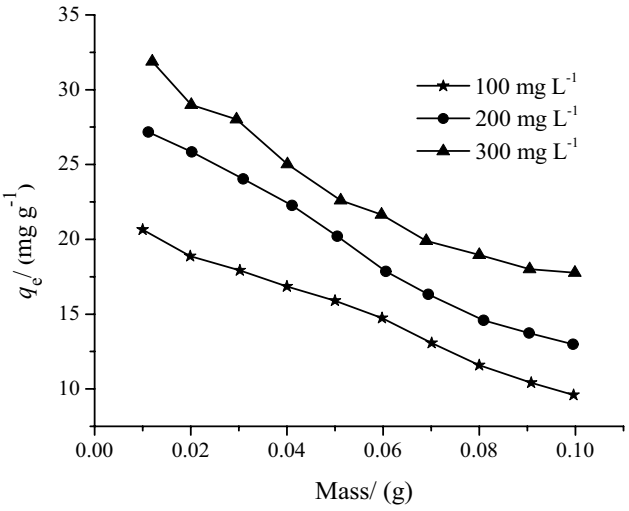

Fig. 8. Effect of Initial MB concentration and adsorbent dose (T = 303 K, t = 8 h, pH = 10).

This feature as well as the ease associated with its use as an adsorbent compensates for the reduction in its adsorption capacity for MB removal and also makes it preferable.

3.2.3. Effect of initial concentration at various dose

The initial concentration of the solution acts as a driving force for the adsorption process as well as increasing the interaction between MB and PN-Fe_3O_4. Fig. 8 illustrates the effect of initial MB concentration on the adsorption process. From the diagram, it was clearly seen that the adsorption process increased with the increase of MB concentration.

3.2.4. Effect of salt

Wastewater has been observed to contain salts hence the effect of ionic strength on the adsorption process is an important factor in the study of adsorption of dyes. In this study, different concentrations of NaCl were employed in order to assess the effect of ionic strength

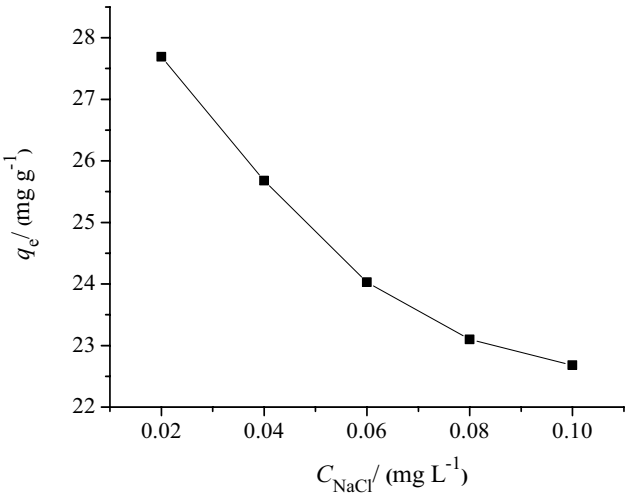

Fig. 9. Effect of NaCl on MB adsorption (C_0 = 300 mg L^{-1}).

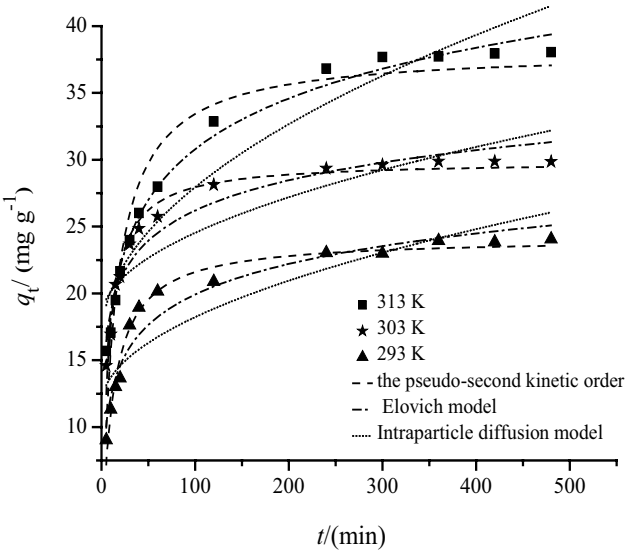

Fig. 10. Effect of contact time on adsorption of MB and fitted kinetic models.

on the adsorption process. As can be seen from Fig. 9, an increase in the concentration of NaCl resulted in the decrease in the value of q_e. This trend could be due to the competitive effect between the positive charge of the salts and that of MB ions for the available sites during the adsorption process [28]. So there was electrostatic attraction or ionic exchange between PN-Fe_3O_4 and MB.

The q_e value at a relatively higher salt concentration (0.1 mol L^{-1}) was observed to have decreased by only 18.41% (i.e., from 27.7 to 22.6 mg g^{-1}). This result implied that other actions (such as hydrogen bond and Van der Waals' force), which were not affected by ionic strength, were existed during the adsorption process. So the ability of PN-Fe_3O_4 can be used in a solution containing salts.

3.2.5. Effect of contact time and kinetic modeling

The results of adsorption quantity per gram PN-Fe_3O_4 (q_t) at different contact time (t) are shown in Fig. 10. It was observed that the adsorption of MB onto PN-Fe_3O_4 increased with an increase in contact time until it reached equilibrium after 4 h. The adsorption rate could be grouped into three phases: an initial rapid phase (before 50 min), an intermediate phase (50–240 min), and a slower phase which resulted in equilibrium (240–480 min). The first phase represented the external surface adsorption. At this stage, there is a diffusion of MB ions from the bulk onto the surface of the adsorbent. This coupled with the availability of adsorption sites acts as a driving force for the adsorption process hence the observation of rapid adsorption [16,17]. The adsorption of MB onto PN-Fe_3O_4 could thus be controlled by an external mass transfer followed by intra-particle diffusion mass transfer. The adsorption process was also observed to be endothermic as q_e values were observed to increase with an increase in temperature.

The adsorption mechanism and characteristics of MB onto PN-Fe_3O_4 were assessed by means of kinetic models. In this regard, the pseudo-second kinetic-order, Elovich equation, and intra-particle diffusion model were used to predict the kinetic process. The pseudo-second-order kinetic model is expressed as [30]:

$$q_t = \frac{k_2 q_e^2 t}{1 + k_2 q_e t} \tag{4}$$

where k_2 refers to the second-order rate coefficient, q_t and q_e are the amounts of MB adsorbed at time t and at equilibrium (mg g^{-1}), respectively.

The Elovich equation is given as [31]:

$$q_t = A + \ln B \tag{5}$$

where A and B are the Elovich constants.

The intra-particle diffusion model is expressed as [32]:

$$q_t = K_{id} t^{1/2} + C \tag{6}$$

where K_{id} is the intra-particle diffusion rate constant and C is the constant.

Table 1 shows the values of the parameters as well as the coefficients of the kinetic models for the adsorption process according to the nonlinear regressive analysis. As shown in Fig. 10, the equilibrium adsorption capacity obtained from the experiment was closer to that obtained from the pseudo-second kinetic-order as compared to the other kinetic models. As shown in Table 1, the R^2 values obtained from the pseudo-second-order kinetic model were relatively greater than that recorded for the Elovich equation and the intra-particle diffusion model. This observation, as well as its smaller recorded SSE values, confirms its suitability to describe the adsorption process. Also, these results suggest that the adsorption process may be a chemical process [13].

3.2.6. Isotherm study

The amount of adsorbed molecules onto the surface of an adsorbent is usually expressed using adsorption

Table 1
Kinetic parameters of MB adsorption onto PN-Fe_3O_4

Pseudo-second-order equation					
T (K)	$q_{m(exp)}$ (mg g^{-1})	$q_{m(theo)}$ (mg g^{-1})	$k_2 \times 10^{-4}$ (g mg^{-1} min^{-1})	R^2	SSE
293	24.1	24.2 ± 0.4	35.2 ± 3.4	0.973	8.19
303	29.9	29.9 ± 0.4	47.9 ± 4.1	0.972	8.45
313	38.1	38.2 ± 1.1	18.5 ± 3.0	0.928	58.7
Elovich model					
T (K)	A	B	R^2	SSE	
293	4.74 ± 1.0	3.30 ± 0.2	0.947	16.3	
303	11.2 ± 1.1	3.26 ± 0.2	0.934	18.5	
313	5.57 ± 0.8	5.48 ± 0.2	0.988	9.68	
Intraparticle diffusion					
T (K)	K_t (mg g^{-1} min$^{-1/2}$)	C (mg g^{-1})	R^2	SSE	
293	0.66 ± 0.1	11.6 ± 1.2	0.794	63.3	
303	0.64 ± 0.1	18.1 ± 1.3	0.763	71.8	
313	1.14 ± 0.1	16.6 ± 1.3	0.907	76.0	

isotherms. The fitting of various isotherm models to that obtained experimentally is very useful in determining the best model which can be used for design purpose. For this experiment, two adsorption isotherm models were applied as shown in Fig. 11.

The Langmuir adsorption isotherm has been successfully applied to many pollutant sorption processes and has been the most widely used sorption isotherm for the sorption of a solute from a liquid solution [33]. It assumes that adsorption takes place at specific homogeneous sites within the adsorbent. The saturated monolayer isotherm can be represented as:

$$q_e = \frac{q_m K_L C_e}{1 + K_L C_e} \tag{7}$$

where q_e is the amount of the MB adsorbed, C_e is the equilibrium concentration of the MB in solution, q_m is the monolayer adsorption capacity and K_L is the Langmuir adsorption constant.

The Freundlich isotherm is also an empirical equation, which assumes that the adsorption takes place on heterogeneous surfaces. The Freundlich equation can be expressed as:

$$q_e = K_F C_e^{1/n} \tag{8}$$

where K_F and $1/n$ are the Freundlich constants related to the adsorption capacity and adsorption intensity of the sorbent, respectively.

The nonlinear regressive method of least sum squares of the difference between calculated data and experimental data was used to determine the isotherm parameters using Origin 8.0 software for the analysis. The isotherm parameters and coefficients of determination (R^2) are shown in Table 2. It was clearly observed from Table 2

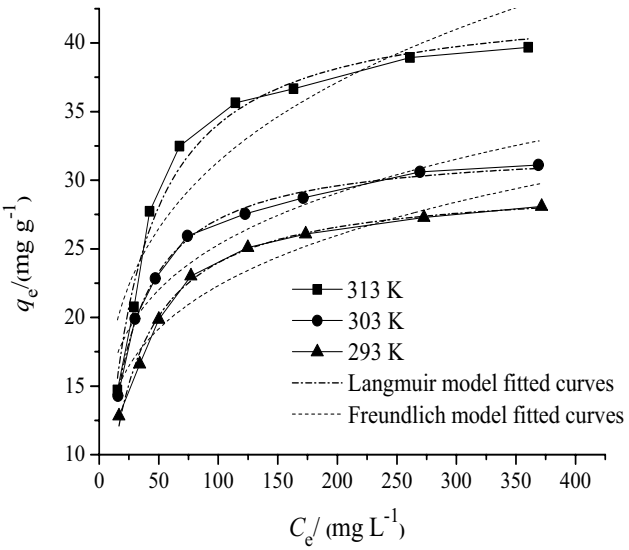

Fig. 11. Adsorption isotherms and fitted curves of MB adsorption onto PN-Fe_3O_4.

that all the R^2 values for the Langmuir isotherm at different temperatures were greater than 0.9. These results show that the adsorption model of MB onto PN-Fe_3O_4 was most favorable toward the Langmuir isotherm as compared to the Freundlich isotherm.

It was also observed from Table 2 that the constants q_m and K_F increased with an increase in temperature. This result indicated that MB can easily be adsorbed onto PN-Fe_3O_4 in aqueous solution [13].

Table 3 is a comparison of results from this study to other adsorbents for the removal of MB. The maximum adsorption capacity of MB on PN-Fe_3O_4 was 32.5 mg g^{-1}. It was shown that the prepared adsorbent in this study

showed significant adsorption capacity and easy separation after the adsorption process. This property makes it practical application in wastewater treatment feasible.

3.2.7. Thermodynamic studies

To estimate the effect of temperature on the adsorption of MB onto PN-Fe_3O_4, the change in free energy change ($\Delta G°$), enthalpy change ($\Delta H°$), and entropy change ($\Delta S°$) were determined. The adsorption process can be summarized which represents a heterogeneous equilibrium. The apparent equilibrium constant (K_c) of the adsorption process is defined as [36]:

$$K_c = \frac{C_{ad,e}}{C_e} \tag{9}$$

where $C_{ad,e}$ is the concentration of MB on the adsorbent at equilibrium (mg L^{-1}). The value of K_c in the lowest experimental MB concentration can be obtained. The value of K_c is used in the following equation to determine the change of Gibbs free energy of adsorption ($\Delta G°$):

$$\Delta G° = -RT\ln K_c \tag{10}$$

Table 2
Parameters of adsorption isotherm models for MB adsorption

Langmuir				
T (K)	q_m (mg g^{-1})	K_L (L mg^{-1})	SSE	R^2
293	29.8 ± 0.4	0.041 ± 0.002	1.41	0.992
303	32.5 ± 0.3	0.050 ± 0.001	0.72	0.996
313	43.0 ± 1.0	0.004 ± 0.003	8.99	0.982
Freundlich				
T (K)	K_F	1/n	SSE	R^2
293	8.12 ± 1.16	0.220 ± 0.003	16.90	0.906
303	10.0 ± 1.4	0.201 ± 0.027	20.53	0.898
313	10.2 ± 2.2	0.244 ± 0.043	76.22	0.845

SSE = $\sum(q-q_c)^2$, q and q_c are values from the experiments and calculation according the model, respectively.

The change of enthalpy ($\Delta H°$) and entropy ($\Delta S°$) can be obtained from the slope and intercept of a van't Hoff equation of $\Delta G°$ vs. T:

$$\Delta G° = \Delta H° - T\Delta S° \tag{11}$$

where $\Delta G°$ is standard Gibbs free energy change, J; R is the universal gas constant, 8.314 J mol^{-1} K^{-1} and T is absolute temperature, K. Values of the standard Gibbs free energy change for the adsorption process obtained from Eq. (10) were presented in Table 4.

The spontaneity of the adsorption of MB onto PN-Fe_3O_4 was confirmed by the negative $\Delta G°$ values. The negative $\Delta G°$ values were observed to decrease with increasing temperature indicating that the spontaneous nature of adsorption of MB were inversely proportional to the temperature and higher temperature favored the adsorption [13].

The positive enthalpy value confirmed the endothermic nature of the adsorption process whereas the obtained $\Delta S°$ value revealed that no significant change occurred in the internal structure of PN-Fe_3O_4 during the adsorption of MB.

3.2.8. Desorption and regeneration studies

The recovery of the adsorbate and the re-use of the adsorbent for further treatment processes is an added advantage of the adsorption process [37–40]. In this regard, desorption of MB from PN-Fe_3O_4-MB were carried out using the following solvents: ethanol, 75% ethanol, 0.01 mol L^{-1} NaOH, 0.1 mol L^{-1} HCl, and 0.1 mol L^{-1} NaCl. The obtained data showed that the percentage of desorption were 73.87%, 34.06%, 74.92%, 8.17%, and 49.25% for 75% ethanol, ethanol, 0.1 mol L^{-1} HCl, 0.01 mol L^{-1} NaOH, and 0.1 mol L^{-1} NaCl, respectively. These results suggest that the adsorption of MB on PN-Fe_3O_4 is not completely reversible and the bonding between the PN-Fe_3O_4 and adsorbed MB is likely to be moderately strong. For the regeneration studies

Table 4
Thermodynamic parameters of MB adsorption on PN-Fe_3O_4

$\Delta H°$ (kJ mol^{-1})	$\Delta S°$ (kJ mol^{-1} K^{-1})	$\Delta G°$ (kJ mol^{-1})		
		293 K	303 K	313 K
0.294	0.08	–0.030	–0.095	–0.248

Table 3
Comparison of the adsorption capacity (q_m) of PN-Fe_3O_4 and other adsorbents for the removal of MB

Adsorbent	q_m (mg g^{-1})	Isotherm	Reference
Peanut husk	72.1	Langmuir	[16]
GO at Fe_3O_4	62.7	Langmuir	[21]
Epichlorohydrin magnetic alginate beads	229	Langmuir	[34]
Modified coffee	74.6	Langmuir	[35]
Modified peanut husk	88.5	Langmuir	[35]
Carboxylic multi-walled carbon nanotubes	120.1	Langmuir	[28]
Magnetic peanut husk	32.5	Langmuir	This paper

of the adsorbent, 0.1 mol L^{-1} HCl was used for desorption. As shown in Fig. 12, the regeneration rate of the adsorbent after three cycles was still high and this suggests that the adsorbent can be reused in some extent.

3.3. Process design for single-stage batch adsorption

Usually, adsorption isotherms can be used to predict the equilibrium result from the isotherm curve and used in the design of a single system in batch adsorption mode [41,42].

The design aim is to reduce initial dye concentration from C_0 to C_e with the same solution volume (L).

The mass balance for MB in the single-stage performance under equilibrium is given by:

$$V\left(C_0 - C_e\right) = m \cdot q_e \tag{12}$$

where m is the amount of added adsorbent (g) and L is MB solution volume (L).

As the Langmuir model is best to describe the equilibrium data, this model is selected to design single-stage adsorption system. According to the Eq. (12) and the Langmuir model, the equation can be arranged as:

$$\frac{m}{V} = \frac{C_0 - C_e}{q_e} = \frac{C_0 - C_e}{q_m K_L C_e / \left(1 + K_L C_e\right)} \tag{13}$$

Fig. 13 represents several plots derived from Eq. (12). These plots showed the predicted adsorbent mass required to remove MB (C_0 = 50 mg L^{-1}) for 60%, 70% 80%, 90%, and 95% removal efficiency for a single-stage batch adsorption system (303 K). Usually, there was more mass with the increase of removal efficiency at the same volume.

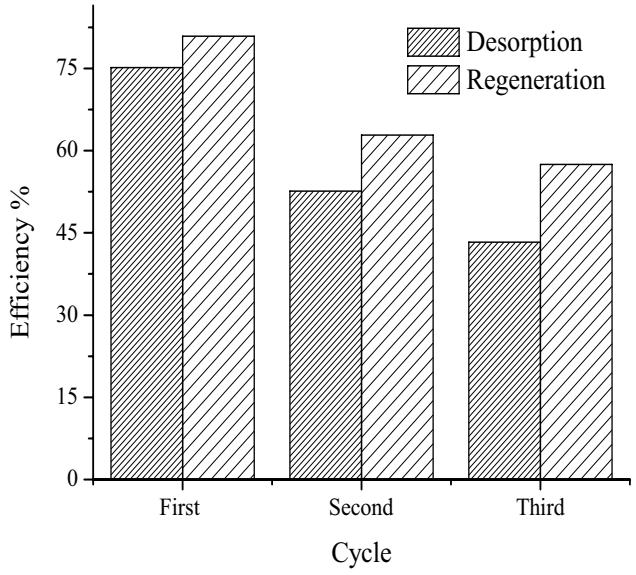

Fig. 12. Desorption/regeneration efficiency of PN-Fe_3O_4 for the removal of MB.

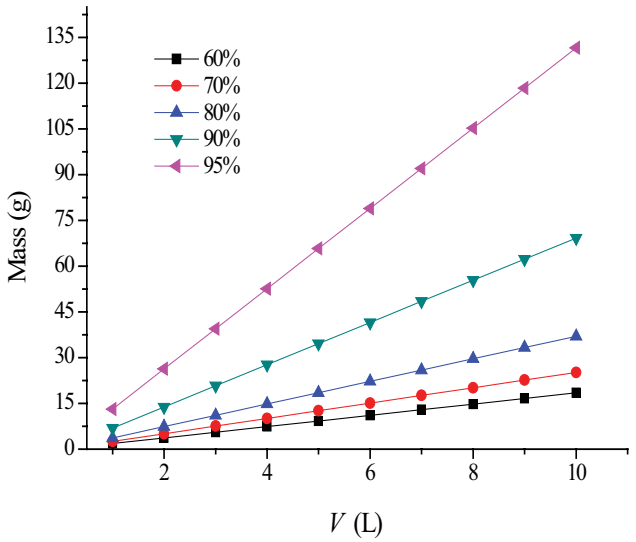

Fig. 13. Adsorbent mass (g) against solution volume (L) (T = 303 K, C_0 = 50 mg L^{-1}).

4. Conclusion

An adsorbent with magnetic characteristics was synthesized using peanut husk, an agricultural waste material, and Fe_3O_4 particles and was used for the adsorption of MB in solution. The results from characterization tests showed the successful magnetization of the peanut husk. The experimental results showed that the adsorption of MB onto PN-Fe_3O_4 was best described by the Langmuir isotherm. The adsorption kinetic process could be divided into three steps, namely, the boundary layer diffusion, followed by the intra-particle diffusion, finally an equilibrium stage. The thermodynamic study indicated that the adsorption reaction was a spontaneous, endothermic, and randomness-increased process. Although the adsorption capacity was relatively lower compared to some studies reported by our group, it still showed a significant adsorption capacity for removal of MB as well as magnetic property which enables it to be easily removed after the adsorption process.

Acknowledgment

This work was supported in part by the Foundation for University Key Teacher by Henan Province (2017GGJS007), the Key Scientific Research Project in Universities of Henan Province (19A150048), and the Outstanding Young Talent Research Fund of Zhengzhou University (1421316038).

References

[1] T.B. Zhou, J. Lu, Y. Zhou, Y.D. Liu, Recent advances for dyes removal using novel adsorbents: a review, Environ. Pollut., 252 (2019) 352–365.
[2] P.S. Kumar, S. Ramalingam, V. Sathyaselvabala, S.D. Kirupha, A. Murugesan, S. Sivanesan, Removal of Cd(II) from aqueous solution by agricultural waste cashew nut shell, Korean J. Chem. Eng., 29 (2012) 756–768.
[3] H. Paudyal, B. Pangeni, K. Inoue, H. Kawakita, K. Ohto, K.N. Ghimire, S. Alam, Adsorptive removal of trace concentration of fluoride ion from water by using dried orange juice residue, Chem. Eng. J., 223 (2013) 844–853.

[4] R. Münze, C. Hannemann, P. Orlinskiy, R. Gunold, A. Paschke, K. Foit, M. Liess, Pesticides from wastewater treatment plant effluents affect invertebrate communities, Sci. Total Environ., 599–600 (2017) 387–399.
[5] W. Li, B.N. Mu, Y.Q. Yang, Feasibility of industrial-scale treatment of dye wastewater via bioadsorption technology, Bioresour. Technol., 277 (2019) 157–170.
[6] L. Vutskits, A. Briner, P. Klauser, E. Gascon, A.G. Dayer, Adverse effects of methylene blue on the central nervous system, Anesthesiology, 108 (2008) 684–692.
[7] P.S. Pamidimukkala, H. Soni, Efficient removal of organic pollutants with activated carbon derived from palm shell: spectroscopic characterisation and experimental optimisation, J. Environ. Chem. Eng., 6 (2018) 3135–3149.
[8] Y. Sun, J.P. Zhang, G. Yang, Z.H. Li, Removal of pollutants with activated carbon produced from K_2CO_3 activation of lignin from reed black liquors, Chem. Biochem. Eng., 20 (2006) 429–435.
[9] M.T. Yagub, T.K. Sen, S. Afroze, H.M. Ang, Dye and its removal from aqueous solution by adsorption: a review, Adv. Colloid Interface Sci., 209 (2014) 172–184.
[10] R.P. Han, L.J. Zhang, C. Song, M.M. Zhang, H.M. Zhu, L.J. Zhang, Characterization of modified wheat straw, kinetic and equilibrium study about copper ion and methylene blue adsorption in batch mode, Carbohydr. Polym., 79 (2010) 1140–1149.
[11] X. Xu, B.Y. Gao, B. Jin, Q.Y. Yue, Removal of anionic pollutants from liquids by biomass materials: a review, J. Mol. Liq., 215 (2016) 565–595.
[12] T. Zhou, W.Z. Lu, L.F. Liu, H.M. Zhu, Y.B. Jiao, S.S. Zhang, R.P. Han, Effective adsorption of light green anionic dye from solution by CPB modified peanut in column mode, J. Mol. Liq., 211 (2015) 909–914.
[13] Y. Shang, J.H. Zhang, X. Wang, R.D. Zhang, W. Xiao, S.S. Zhang, R.P. Han, Use of polyethyleneimine-modified wheat straw for adsorption of Congo red from solution in batch mode, Desal. Water Treat., 57 (2015) 8872–8883.
[14] W.S. Wan Ngah, M.A.K.M. Hanafiah, Removal of heavy metal ions from wastewater by chemically modified plant wastes as adsorbents: a review, Bioresour. Technol., 99 (2008) 3935–3948.
[15] R.D. Zhang, J.H. Zhang, X.N. Zhang, C.C. Dou, R.P. Han, Adsorption of Congo red from aqueous solutions using cationic surfactant modified wheat straw in batch mode: kinetic and equilibrium study, J. Taiwan Inst. Chem. Eng., 45 (2014) 2578–2583.
[16] J.Y. Song, W.H. Zou, Y.Y. Bian, F.Y. Su, R.P. Han, Adsorption characteristics of methylene blue by peanut husk in batch and column modes, Desalination, 265 (2011) 119–125.
[17] Y.F. Gu, M.Y. Liu, M.M. Yang, W.L. Wang, S.S. Zhang, R.P. Han, Adsorption of light green anionic dye from solution using polyethyleneimine-modified carbon nanotubes in batch mode, Desal. Water Treat., 138 (2019) 368–378.
[18] P. Xu,. M. Zeng, D.L. Huang, C. Feng, S. Hu, M.H. Zhao, Z.F. Liu, Use of iron oxide nanomaterials in wastewater treatment: a review, Sci. Total Environ., 424 (2012) 110–120.
[19] R. Sivashankar, A.B. Sathya, K. Vasantharaj, V. Sivasubramanian, Magnetic composite an environmental super adsorbent for dye sequestration – a review, Environ. Nanotechnol. Monit. Manage., 1–2 (2014) 36–49.
[20] B. Jiang, L. Lian, Y. Xing, N.N. Zhang, Y.T. Chen, P. Lu, D.Y. Zhang, Advances of magnetic nanoparticles in environmental application: environmental remediation and (bio) sensors as case studies, Environ. Sci. Pollut. Res., 25 (2018) 30863–30879.
[21] M.Y. Liu, J.J. Dong, W.L. Wang, M.M. Yang, Y.F. Gu, R.P. Han, Study of methylene blue adsorption from solution by magnetic graphene oxide composites, Desal. Water Treat., 147 (2019) 398–408.
[22] Y.Y. Hu, R.P. Han, Selective and efficient removal of anionic dyes from solution by zirconium(IV) hydroxide coated magnetic materials, J. Chem. Eng. Data, 64 (2019) 791–799.
[23] S. Laurent, D. Forge, M. Port, A. Roch, C. Robic, L.V. Elst, Magnetic iron oxide nanoparticles: synthesis, stabilization, vectorization, physicochemical characterizations, and biological applications, Chem. Rev., 108 (2008) 2064–2110.
[24] J. Zhou, Y. Liu, X. Zhou, J. Ren, C. Zhong, Removal of mercury ions from aqueous solution by thiourea-functionalized magnetic biosorbent: preparation and mechanism study, J. Colloid Interface Sci., 507 (2007) 107–118.
[25] X. Zhou, J. Zhou, Y. Liu, J. Guo, J. Ren, F. Zhou, Preparation of iminodiacetic acid-modified magnetic biochar by carbonization, magnetization and functional modification for Cd(II) removal in water, Fuel, 233 (2018) 469–479.
[26] Y. Zong, H. Xin, J. Zhang, X. Li, F. Feng, X. Deng, One-pot, template- and surfactant-free solvothermal synthesis of high-crystalline Fe_3O_4 nanostructures with adjustable morphologies and high magnetization, J. Magn. Magn. Mater., 423 (2017) 321–326.
[27] J. Liu, Y. Yu, S. Zhu, J. Yang, J. Song, W. Fan, Synthesis and characterization of a magnetic adsorbent from negatively-valued iron mud for methylene blue adsorption, PLoS One, 13 (2018) e0191229.
[28] M.M. Yang, X.Y. Li, W.L. Wang, S.S. Zhang, R.P. Han, Adsorption of methyl blue from solution by carboxylic multi-walled carbon nanotubes in batch mode, Desal. Water Treat., 159 (2019) 365–376.
[29] B. Volesky, Biosorption and me, Water Res., 41 (2007) 4017–4029.
[30] Y.S. Ho, G. McKay, Pseudo-second-order model for sorption process, Process Biochem., 34 (1999) 451–465.
[31] C.W. Cheung, J.F. Porter, G. McKay, Sorption kinetics for the removal of copper and zinc from effluents using bone char, Sep. Purif. Technol., 19 (2000) 55–64.
[32] W.J. Weber Jr., J.C. Morris, Kinetic of adsorption on carbon from solution, J. Sanitary Eng. Div., 89 (1962) 31–59.
[33] I. Langmuir, The constitution and fundamental properties of solids and liquids, J. Am. Chem. Soc., 38 (1916) 2221–2295.
[34] V. Rocher, A. Bee, J.M. Siaugue, V. Cabuil, Dye removal from aqueous solution by magnetic alginate beads crosslinked with epichlorohydrin, J. Hazard. Mater., 178 (2010) 434–439.
[35] N. Besharati, N. Alizadeh, S. Shariati, Removal of cationic dye methylene blue (MB) from aqueous solution by coffee and peanut husk modified with magnetite iron oxide nanoparticles, J. Mex. Chem. Soc., 62 (2018) 110–124.
[36] Z. Aksu, Determination of the equilibrium, kinetic and thermodynamic parameters of the batch biosorption of nickel(II) ions onto *Chlorella vulgaris*, Process Biochem., 38 (2002) 89–99.
[37] R.P. Han, Y. Wang, Q. Sun, L.L. Wang, J.Y. Song, X.T. He, C.C. Dou, Malachite green adsorption onto natural zeolite and reuse by microwave irradiation, J. Hazard. Mater., 175 (2010) 1056–1061.
[38] B.L. Zhao, W. Xiao, Y. Shang, H.M. Zhu, R.P. Han, Adsorption of light green anionic dye using cationic surfactant-modified peanut husk in batch mode, Arabian J. Chem., 10 (2017) S3595–S3602.
[39] Y.F. Gu, M.M. Yang, W.L. Wang, R.P. Han, Phosphate adsorption from solution by zirconium loaded carbon nanotubes in batch mode, J. Chem. Eng. Data, 64 (2019) 2849–2858.
[40] Y.N. Shang, X. Xu, B.Y. Gao, Q.Y. Yue, Highly selective and efficient removal of fluoride from aqueous solution by Zr-La dual-metal hydroxide anchored bio-sorbents, J. Cleaner Prod., 199 (2018) 36–46.
[41] S. Dawood, T.K. Sen, Removal of anionic dye Congo red from aqueous solution by raw pine and acid-treated pine cone powder as adsorbent: equilibrium, thermodynamic, kinetics, mechanism and process design, Water Res., 46 (2012) 1933–1946.
[42] S.S. Chen, K. Wen, X.T. Zhang, R.Z. Zhang, R.P. Han, Adsorption of Neutral red onto MIL-100(Fe) from solution: characterization, equilibrium, kinetics, thermodynamic and process design, Desal. Water Treat., 177 (2020) 197–208.